

On the Markovian assumption in near-wall turbulence: The case of particle resuspension

David Ben-Shlomo^{1,2}, Ronen Berkovich^{1,3,*}, Eyal Fattal^{2,*}

¹Department of Chemical Engineering, Ben-Gurion University of the Negev, Beer-Sheva 8410501, Israel

²Department of Applied Mathematics, Israel Institute for Biological Research, Ness-Ziona 7410001, Israel

³Ilze Katz Institute for Nanoscience and Technology, Ben-Gurion University of the Negev, Beer-Sheva 8410501, Israel

* Corresponding authors.

E-mail address: berkovir@bgu.ac.il (R. Berkovich); eyalf@iibr.gov.il (E. Fattal).

ABSTRACT

We investigate the validity of the Markovian assumption in modeling near-wall turbulence by analyzing the detachment of micron-sized particles from the viscous sublayer. By coupling direct numerical simulations with a fractional Ornstein-Uhlenbeck process, we demonstrate that while wall shear stress events follow Poissonian occurrence statistics, their internal dynamics exhibit strong temporal persistence (Hurst exponent $H \approx 0.84$), indicating non-Markovian memory. We reveal that the successful predictions of Markovian resuspension models stems from their free parameter acting as a phenomenological surrogate for flow memory. We further identify a critical regime transition governed by a wall shear stress events decay rate, λ . We identify a strong intermittency regime ($\lambda < 0.2$), where coherent structures exhibit extended temporal correlations that cannot be mimicked by white noise. Conversely, rapid decays ($\lambda > 0.2$) generate quasi-random fluctuations that justify the Markovian approximation. These findings offer a new perspective on the physical validity of classical stochastic modeling in wall-bounded flows.

Keywords: Stochastic modeling, Near-wall turbulence, Coherent structures, Resuspension.

1. Introduction

Turbulence modeling remains one of the most challenging goals in modern physics, particularly with wall-bounded flows where strong inhomogeneity and anisotropy complicate universal scaling [1]. While the Kolmogorov-Obukhov 1941 (K41) [2], [3] theory provides robust descriptions for homogeneous, isotropic turbulence in the infinite Reynolds number limit, its applicability to the near-wall region, dominated by coherent structures, is limited. Finding a more general and valid theoretical framework to these turbulent regimes is critical for providing modeling descriptions of processes like particle resuspension, where the detachment mechanism for particles fully immersed in the viscous sublayer (with dimensionless diameters smaller than five wall units, $d_p^+ < 5$) remains unresolved [4], [5], [6].

There are two main approaches for modeling the driving force of detachment. One approach attributes detachment to particle-surface interactions (e.g., collisions with asperities) [7], [8], [9]. The other points to particle-fluid interactions driven by near-wall coherent structures. While early hypotheses by Sutherland [10] and Cleaver & Yates [11] proposed that turbulent bursts could directly lift particles, later findings that detachment is preceded by rolling [12], [13], [14] complicated this view. Consecutive investigations have produced contrasting results. Some experiments suggest bursting has negligible impact due to small uplift angles [15], while others, including direct numerical simulations (DNS), explicitly link detachment to sweep and ejection events [16], [17], [18], [19] [20], [21]. Nevertheless, theoretical models have struggled to resolve the physical mechanism linking these coherent structures to resuspension. As van Hout stated, “*Particularly within the field of particle resuspension, most of the theoretical works seems to neglect the incorporation of the actual physical mechanism linking coherent structures with resuspension*” [18].

To address this, one must consider the flow structure. The viscous sublayer ($y^+ < 5$, where $y^+ = \frac{yu_\tau}{\nu}$ denotes the dimensionless wall-normal coordinate, u_τ is the friction velocity and ν is the kinematic viscosity) is not laminar but consists of alternating high- and low-velocity streaks exhibiting significant temporal persistence [22], [23] [24]. Quadrant analysis [25] [26], identifies these coherent motions as ejections (Q2) and sweeps (Q4), which dominate turbulence production and manifest as low- and high-drag events, respectively [27]. Furthermore, recent high-resolution DNS and experimental studies [28] [29], [30], [31] confirm that the sublayer hosts rare, intense intermittent events (e.g., backflow) originating from multi-scale interactions. Importantly, the existence of precursor signatures for these events implies that near-wall fluctuations are not random, independent increments, but organized sequences with distinct temporal correlations.

We hypothesize that this structural intermittency governs the high-order fluctuations responsible for particle detachment. However, existing stochastic models [9], [32], [33], [34] predominantly rely on the classical K41 theory, modeling velocity fluctuations as a Markovian process. This assumes that velocity increments, $\Delta u(t)$, become uncorrelated over time (i.e., the flow has no "memory"). While being justified for some free shear flows [35], [36], [37] this assumption is questionable in the viscous sublayer where persistent coherent structures induce spatial and temporal correlations. Nevertheless, previous Markovian models often achieve good reconstruction of experimental data by fitting free parameters (associated with particle-surface or particle-flow interactions) to the measurements, potentially masking the underlying mechanism of the process.

In the present work, we investigate whether the Markovian assumption is physically justified in the near-wall region. We analyze DNS data to characterize the

memory of the flow and introduce a generalized non-Markovian stochastic framework. Consistent with the refined Kolmogorov theory (1962) for intermittent turbulence (K62) [38], this model explicitly links the statistics of particle detachment to the persistent dynamics of coherent structures.

2. Theory and methodology

As discussed in the introduction, near-wall coherent structures manifest as high- and low-drag events in the turbulent boundary layer [39], [40]. Crucially, the persistent nature of these structures suggests that the forces acting on a particle are not random, but exhibit significant temporal correlations. Accordingly, we focus on characterizing the timescales, amplitudes, and memory properties of these events to link particle motion in the viscous sublayer to the underlying flow topology.

2.1 Analysis of high- and low-drag events in the viscous sublayer

We analyze data from the John Hopkins Turbulent Database (JHTDB) for a fully developed turbulent channel flow ($Re_\tau \approx 1,000$) [41], [42]. The simulation domain covers $8\pi h \times 2h \times 3\pi h$ (in the streamwise x , wall normal y , and spanwise z directions, respectively; where h is the channel half-height) fully resolving scales from energy-containing eddies down to the dissipative Kolmogorov scales. Given that the stochastic resuspension framework is formulated as a single-particle model, the particle concentration is assumed to be sufficiently dilute so that its influence on the carrier-phase flow remains negligible, consistent with the one-way coupling regime [43], [44]. This is supported by findings that particle and fluid velocity fluctuations in the sublayer are of comparable magnitude, implying minimal feedback [45]. Thus, the DNS velocity field is used as a prescribed input.

2.1.1 Identification of high- and low-drag events

We identify events using an amplitude criterion based on the normalized wall shear stress (WSS), expressed as the ratio between the instantaneous WSS and its time-averaged value, $\tau_w/\langle\tau_w\rangle$. An amplitude criterion is adopted, where events are classified as high- or low-drag when the normalized WSS exceeded a $\pm 5\%$ threshold. This value was chosen over larger thresholds (e.g., $\pm 10\%$) as it increases the number of detected events, thereby improving the robustness of the subsequent statistical analysis [46], [47]. A recent research demonstrated that adopting inner scaling ($\Delta t^+ = \Delta t u_\tau^2 / \nu$) renders the fraction of time spent in high- and low-drag events independent of the friction Reynolds number Re_τ [27]. Based on this finding, we employed inner time scaling in our analysis. A minimum duration criterion was not applied, consistent with other study [47], due to the short characteristic timescales of events in the viscous sublayer.

2.1.2 Time-correlation analysis

To quantify the long-range temporal correlations (i.e., memory effects) in the WSS signal, the Hurst exponent (H) was estimated. While several methods for calculating the Hurst exponent exist (e.g., Rescaled Range (R/S), Aggregate Variance (AV), Detrended Fluctuation Analysis (DFA)) [48], [49], [50], we adopted the R/S analysis. This method was chosen for its extensive use and demonstrated robustness, particularly compared to methods like DFA which can yield unreliable H values for shorter time series [50], [51].

2.2 Lagrangian stochastic particle resuspension models

2.2.1 Markovian model

Our non-Markovian generalization builds upon the Lagrangian stochastic Markovian model of Ben Shlomo et al. [32]. It assumes the particle rolls in a single direction [4], [12], [52], [53], governed by the moment balance, M , about a pivot point:

$$M \equiv I \frac{d\omega}{dt} = bF_D + \frac{a}{2}F_L - r_a F_{adh} - \frac{a}{2}mg \quad (1)$$

where I is the particle moment of inertia, approximated as a sphere and evaluated using the parallel axis theorem $I = \frac{7}{20}md_p^2$, d_p is the particle diameter, m is the particle mass, g is the gravitational acceleration, ω is the particle angular velocity, a is the distance between consecutive surface asperities, r_a is the lever arm of the adhesion force, and $b = \sqrt{\left(\frac{d_p}{2}\right)^2 - \left(\frac{a}{2}\right)^2}$. The hydrodynamic forces F_D (drag) and F_L (lift) are modeled using Stokesian drag [54] with O'Neill's wall-correction [55] and the formulation of Mollinger & Nieuwstadt [56] combined with Maude's wall-correction factor [57], respectively. The mean adhesion force F_{adh} is calculated using the Rabinovich expression [58], which describes the interaction potential between a spherical particle and a rough surface.

In this framework, the total angular velocity ω is separated into mean and fluctuating components. The mean component is determined from the forces in Equation (1), while the fluctuating component ω' is modeled as a stochastic process. Consistent with K41 theory [45], this model uses a standard Ornstein-Uhlenbeck process (OUP) [59], [60]:

$$d\omega'(t) = -\omega'(t) \frac{dt}{T} + \sqrt{\frac{2\sigma^2}{T}} dW(t) \quad (2)$$

where T is the integral timescale of the OUP, σ is a parameter related to the variance and the autocorrelation of the process, and $W(t)$ denotes a Wiener process [59]. When the particle's kinetic energy exceeds a critical threshold, such that $\omega > \omega_c = 2a/(d_p\Delta t)$ (where Δt is the simulation time-step), the surface adhesion energy is overcome. At this point, the particle is considered to lose its interaction with the surface and becomes resuspended. It is important to highlight that according to Fu et al. [33],

the constant σ depends on a free model parameter, C_0 . As they note, “*The exact physical meaning of the model constant C_0 is not known, but it should be related to the integral time scale of the fluctuating moment.*” We assume that the physical meaning of this constant can be linked with the intermittent dynamics in the viscous sublayer, induced by coherent structures. We further explore this relation in the following section. While demonstrating good agreement with experimental observations [32], this model’s Markovian (memoryless) assumption cannot capture the persistent temporal correlations from coherent structures.

2.2.2 Non-Markovian model

The findings that intermittent coherent structures penetrate down to the viscous sublayer, seems to contradict the assumption of uncorrelated white noise, as it may not adequately capture the inhomogeneous dynamics of near-wall turbulence. Faranda et al. [61] demonstrated that Hurst exponents provide a useful measure of deviations from the K41-based Markovian description in inhomogeneous and anisotropic turbulent flows, linking these deviations to the presence of intermittent coherent structures. Accordingly, we propose a generalized non-Markovian model. The standard OUP is replaced with a fractional Ornstein–Uhlenbeck process (fOUP) [62], a formulation consistent with the refined K62 theory [38]. This is achieved by changing the Wiener process increment $dW(t)$ in equation (2) to a fractional Brownian motion (fBm) increment, $dB^H(t)$. The governing stochastic differential equation for the fluctuating component becomes

$$d\omega'(t) = -\omega'(t) \frac{dt}{T} + \sqrt{\frac{2\sigma^2}{T}} dB^H(t) \quad (3)$$

Here, the Hurst exponent H (estimated from DNS data in section 3.1) governs the memory of the process. For $H = 0.5$, the standard Wiener process is recovered. For $0.5 < H < 1$, the process exhibits long-range temporal correlations, and for $H < 0.5$, it exhibits short-range temporal correlations.

$< H < 1$, the process is persistent, with trends tending to continue in the same direction, thus reflecting the influence of coherent structures [61], [63], [64], [65]. The fBm can be represented as a cumulative integral of a Gaussian random process:

$$B^H(t) = \frac{1}{\Gamma(H + \frac{1}{2})} \int_{-\infty}^0 \left[(t-s)^{H-\frac{1}{2}} - (-s)^{H-\frac{1}{2}} \right] dW(s) + \frac{1}{\Gamma(H + \frac{1}{2})} \int_0^t (t-s)^{H-\frac{1}{2}} dW(s) \quad (4)$$

where $\Gamma(H)$ is the gamma function [66]. We further note that, although the fOUP is a generalized form of the OUP by incorporating non-Markovian memory effects, the one-point statistics of both processes satisfy the same general form of the Fokker-Planck equation (also known as the forward Kolmogorov equation) [67]:

$$\frac{\partial}{\partial t} P(\omega', t | \omega'_0, t_0) = \left(-\frac{\partial}{\partial \omega'} D_1(\omega', t) + \frac{\partial^2}{\partial \omega'^2} D_2(\omega', t) \right) P(\omega', t | \omega'_0, t_0) \quad (5)$$

where $P(\omega', t | \omega'_0, t_0)$ is the conditional PDF (with $t > t_0$), $D_1(\omega', t)$ is the drift coefficient and $D_2(\omega', t)$ is the diffusion coefficient. While the structural form of equation (5) is identical for both models, the memory effects in the fOUP are encapsulated in a time-dependent diffusion coefficient, $D_2 \sim t^{2H-1}$, contrasting with the constant diffusion of the standard OUP. Further details on the effect of the Hurst parameter on particle dynamics and the numerical algorithm of the non-Markovian model can be found in the supplementary materials.

3. Results and discussion

3.1 DNS analysis

As outlined in the previous section, a DNS analysis was conducted to characterize the spatio-temporal properties of high- and low-drag events within the viscous sublayer. Figure 1 presents the normalized fluctuating WSS as a function of inner-scaled time. Data were sampled at four spatial locations in the streamwise and spanwise directions, specifically $(2\pi, 0.5\pi)$, $(4\pi, 1.5\pi)$, $(6\pi, 2.5\pi)$, and $(7\pi, 2\pi)$, and at

$0.5 < y^+ < 1.5$ in the wall-normal direction, corresponding to the lower portion of the viscous sublayer [68]. At each time point where the normalized WSS exceeded the $\pm 5\%$ threshold relative to the mean, a high- or low-drag event was identified and recorded for subsequent analysis. As shown in figure 1, the viscous sublayer exhibits substantial shear fluctuations, deviating up to 10% from the mean, consistent with previous observations [69], [70]. These excursions are not merely random noise, as they represent the footprint of persistent coherent structures that penetrate into the viscous sublayer [31], [71], [72]. The identification of discrete high- and low-drag events (marked in red and blue) confirms that the particle experiences the flow as a sequence of distinct forcing intervals rather than a continuous mean flow. Collectively, these results support the adoption of a time-correlated, non-Markovian modeling framework to capture the near-wall flow dynamics in the viscous sublayer.

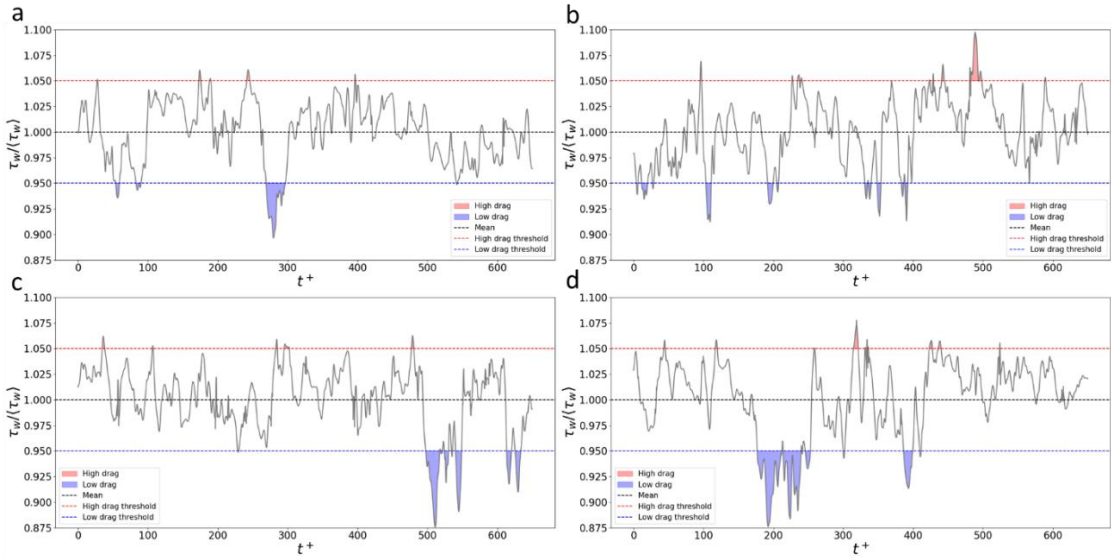


Fig. 1. Normalized fluctuating WSS at four locations in the streamwise and spanwise directions within the channel: (a) $(2\pi, 0.5\pi)$, (b) $(4\pi, 1.5\pi)$, (c) $(6\pi, 2.5\pi)$ and (d) $(7\pi, 2\pi)$, as a function of inner-scaled time. Data were sampled within the viscous sublayer $0.5 < y^+ < 1.5$. High-drag events (red) and low-drag events (blue) are whenever the threshold criterion is exceeded.

Subsequently, the PDF of the duration and frequency of high- and low-drag events were computed by extending the analysis performed for figure 1 to 100 distinct spatial locations in the streamwise-spanwise plane within the viscous sublayer. Figure 2 portrays the resulting PDFs of event durations alongside histograms of the time intervals between consecutive events. Furthermore, an exponential function of the form $P(\Delta t^+) = Ae^{-\lambda\Delta t^+}$, where A is the amplitude and λ is the decay rate, was fitted to each distribution. We note that since the time variable is inner-scaled (and thus dimensionless), the resulting decay rate is likewise dimensionless.

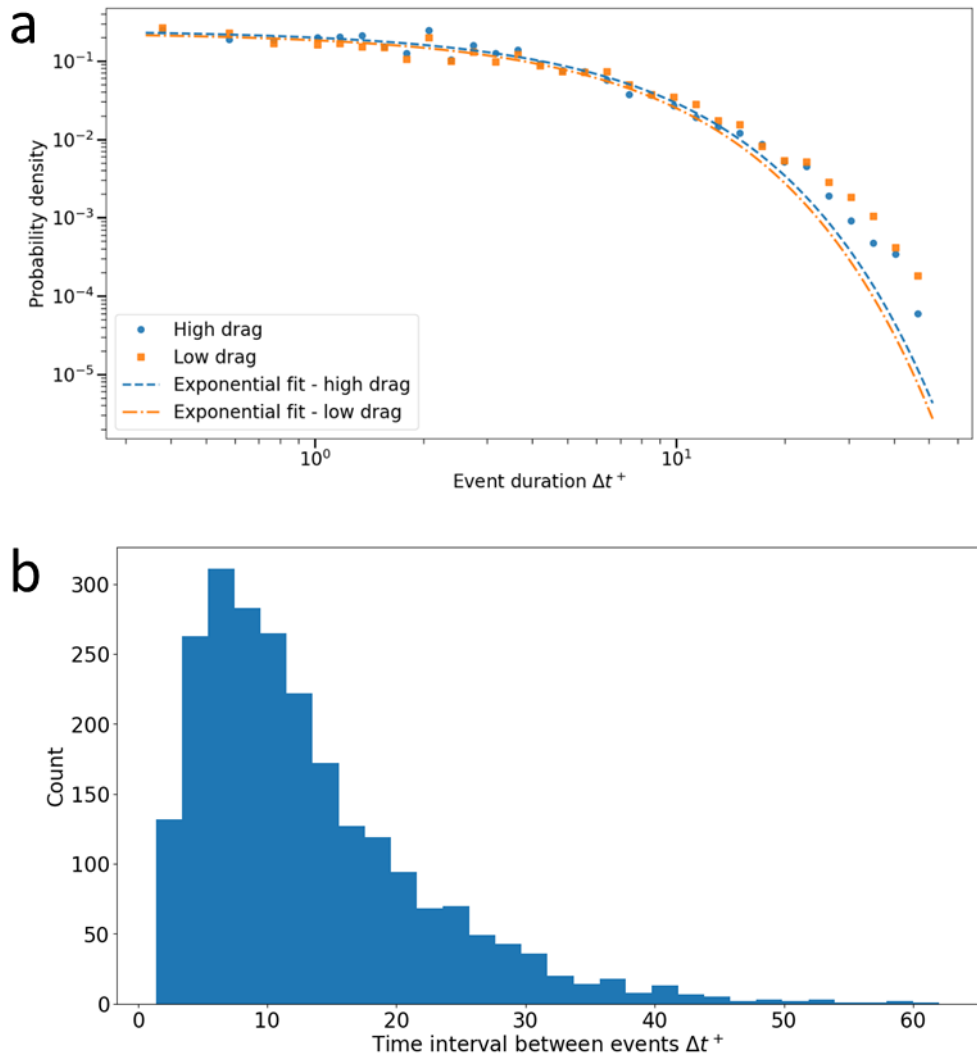


Fig. 2. (a) PDFs of high-drag (blue circles) and low-drag (orange squares) events durations within the viscous sublayer, with corresponding exponential fits shown for high-drag events (blue dashed line) and low-drag events (orange dash-dotted line). (b) Histogram of the time interval between consecutive events. Both PDFs and histograms were obtained from analyses at 100 distinct spatial locations in the streamwise-spanwise plane within $0.5 < y^+ < 1.5$.

As illustrated in figure 2(a), the probability of an event persisting decays exponentially with its duration. Both PDFs are well described by the exponential relationship. This behavior is characteristic of a Poisson process, implying that the termination of a drag event is a random, memoryless occurrence. However, a crucial distinction should be made: while the switching between events follows Poissonian statistics (random occurrence), the dynamics during an event are governed by the structure itself, which implies strong temporal correlation. Table 1 summarizes the exponential fit parameters. Notably, the decay rates obtained here ($\lambda \approx 0.2$) are approximately one order of magnitude higher than those reported by Agrawal et al. [27]. This discrepancy likely stems from the differing threshold criteria. Agrawal et al. employed a strict time-duration filter ($t^+ > 200$), effectively isolating the larger structures, whereas our analysis captures the spectrum of sublayer events relevant to the short timescales of particle resuspension. The histogram of the time intervals between consecutive events (figure 2(b)), where high- and low-drag events are counted together, shows that, based on 2,354 detected events (counts), the median interval is $10.8\Delta t^+$ and the mean interval is $13.2\Delta t^+$. These findings are consistent with previous numerical and experimental studies, which reported that the average spacing between near-wall velocity spikes is typically less than $20\Delta t^+$ [73], [74].

Table 1 Amplitude (A) and decay rate (λ) of high- and low-drag events within the viscous sublayer at $Re_\tau \approx 1,000$, including their standard error. The goodness of fit (R^2) to the exponential function is indicated in brackets next to each event type.

Event type	A	λ
High drag (0.93)	0.2231 ± 0.0113	0.2026 ± 0.0217
Low drag (0.90)	0.2391 ± 0.0149	0.2391 ± 0.0298

To investigate the non-Markovian characteristics of the viscous sublayer flow, a time-correlation analysis was conducted with the aim of quantifying the degree of temporal correlation and extracting the Hurst exponent from DNS data. This was accomplished using the R/S analysis, as described in section 2.1.2. In the present study, the R/S method was applied to the temporal evolution of the wall-normal shear stress, $\tau_w(t)$, sampled within $y^+ \in (0.5, 1.5)$. The sample length, n , defines a temporal window over which the near-wall turbulent fluctuations are evaluated. For each block of length n , the adjusted range R is computed as the difference between the maximum and minimum of the cumulative deviation from the block mean, capturing the largest persistent excursion of the shear stress relative to the local average. The standard deviation S represents the root-mean-square magnitude of the fluctuations within the same window, reflecting the local turbulent intensity. The ratio R/S thus provides a normalized measure of persistence relative to fluctuation strength, and its scaling with n yields the Hurst exponent H , which characterizes the temporal correlation and memory of the near-wall turbulent structures.

Figure 3 portrays the Hurst exponent estimation from wall-shear-stress time series obtained from the DNS using R/S analysis. Figure 3(a) presents a representative

R/S calculation for a single spatial location (channel center), while figure 3(b) displays a heat map of Hurst values computed at 100 spatial locations across the channel. The Hurst exponent varies between 0.79 and 0.87 with median $H_{med} = 0.84$ and mean $\bar{H} = 0.83$. These values indicate pronounced long-range temporal correlations and strong persistence in the near-WSS signal, supporting a non-Markovian description of the turbulent fluctuations in the viscous sublayer.

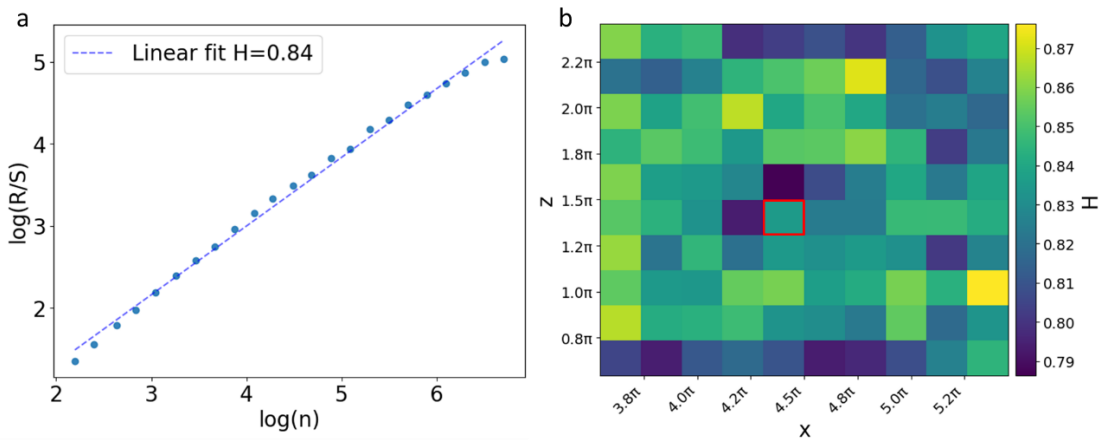


Fig. 3. Estimation of the Hurst exponent using rescaled range analysis. (a) Example for a single point located at the channel center in the streamwise and spanwise directions ($4\pi, 1.5\pi$) and within $0.5 < y^+ < 1.5$. According to the R/S method, the slope of the linear fit yields a Hurst exponent of $H = 0.84$. (b) Heat map of Hurst exponent values computed from 100 spatial locations across the channel. The data point shown in (a) is indicated by a red square outline in (b).

3.2 Resuspension models simulations

Following the characterization of flow dynamics within the viscous sublayer and the integration of extracted timescales and correlation intensities into the non-Markovian resuspension model, we address a fundamental theoretical question: given that the viscous sublayer is demonstrably non-Markovian ($H \approx 0.84$), why do classical Markovian resuspension models [9], [32], [33], [34] often succeed in reconstructing

experimental data? To resolve this, we investigate whether the free parameter in the Markovian model, C_0 , serves as a theoretical representation for the missing physics of flow memory.

Comparative numerical simulations were performed using both the non-Markovian and Markovian frameworks, tracking tungsten particles ($d_p = 13 \mu\text{m}$) on a hydrodynamically smooth surface (with root mean square roughness of 2.2 nm), ensuring full immersion in the viscous sublayer. Other model parameters not explicitly detailed here are specified in [32]. In the non-Markovian model, the event decay rate λ was varied to test the sensitivity of the system to intermittency, while in the Markovian model, the parameter C_0 which scales the stochastic forcing variance and is theoretically linked to the integral timescale of turbulent fluctuations, was systematically varied.

Figure 4(a) illustrates the sensitivity of the Markovian model to C_0 . When C_0 approaches zero, the stochastic contribution vanishes, and resuspension is driven solely by mean forces, resulting in under-prediction. Crucially, we observe that when C_0 is set to $1 \cdot 10^{-3}$, the specific value empirically calibrated by Fu et al. [33] to match experimental measurements, the Markovian prediction aligns with our non-Markovian model. This alignment suggests a major physical insight: For the specific conditions of the viscous sublayer, the non-Markovian and Markovian descriptions can yield equivalent macroscopic results, but through different theoretical pathways. The non-Markovian model achieves this through explicit analysis of drag event structures (H , λ), whereas the Markovian model achieves this through the calibration of C_0 . Therefore, we postulate that C_0 acts not merely as a fitting constant, but as a phenomenological surrogate for the integrated memory of high- and low-drag events. By tuning C_0 , previous studies effectively adjusted the energy of the white noise to mimic the persistence of coherent structures.

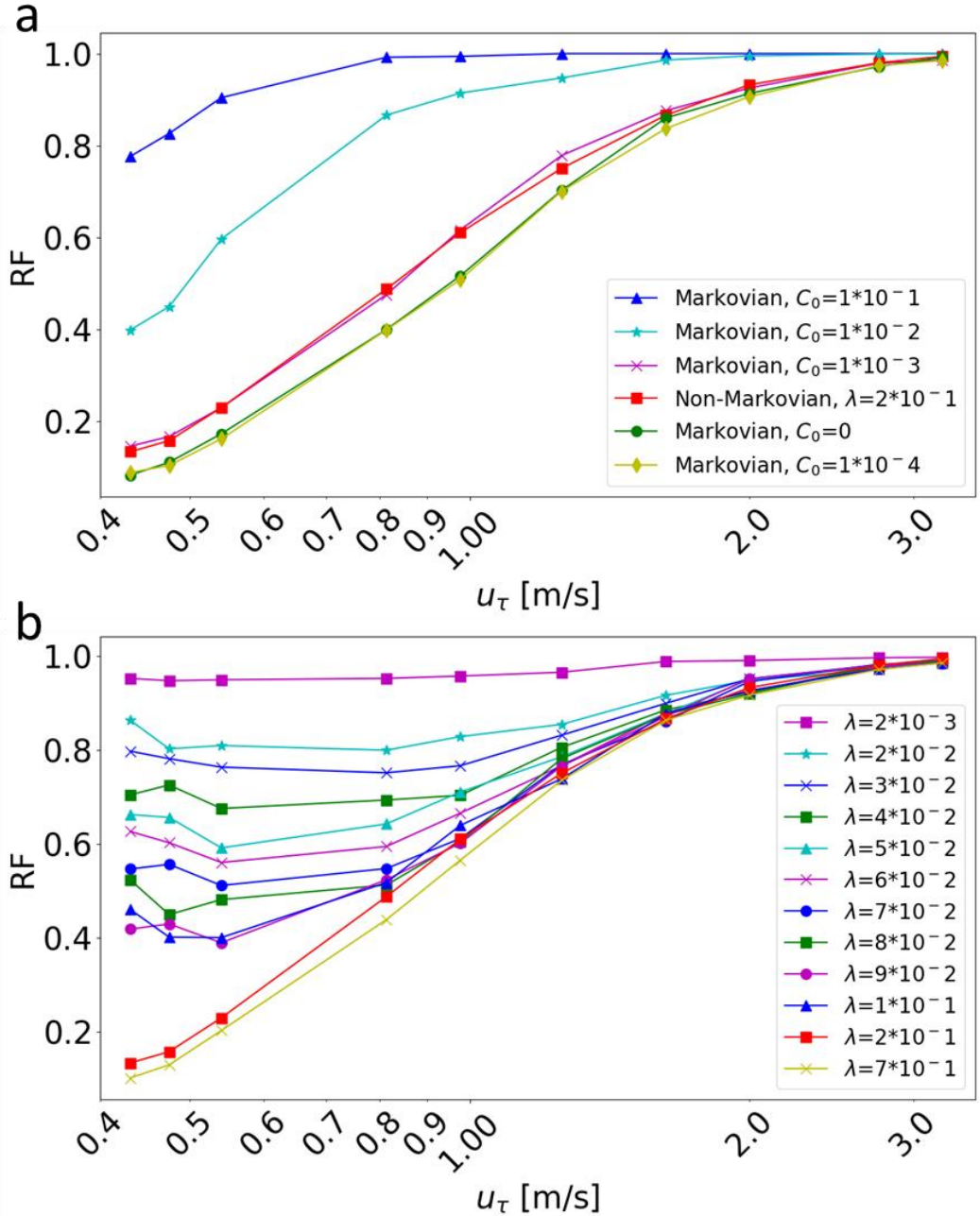


Fig. 4. Resuspension fraction (RF) as a function of friction velocity for particles fully immersed within the viscous sublayer. (a) Comparison of the Markovian model (varying C_0) and the non-Markovian model ($\lambda = 0.2$) predictions. (b) Non-Markovian model predictions for varying high- and low-drag events decay rates, λ .

To define the limits of this equivalence, Figure 4(b) analyzes the effect of the event decay rate, λ , on resuspension. We identify a distinct regime transition around a

critical threshold of $\lambda \approx 0.2$. In the strong intermittency regime ($\lambda < 0.2$), where events are long-lived, the resuspension profile exhibits a characteristic plateau at low friction velocities ($u_\tau < 1$ m/s). This regime is strongly non-Markovian, as the flow memory is sufficiently long that the particle experiences sustained forcing, leading to dynamics that cannot be mimicked by the white noise approximation shown in figure 4(a). Notably, the Markovian model fails to capture the characteristic plateau behavior observed in this regime, regardless of the calibration of C_0 . Conversely, in the weak intermittency regime ($\lambda > 0.2$), events become shorter and more frequent, causing the plateau to disappear and the curve to smooth out. In this limit, the coherent structures decay so rapidly that, from the particle's perspective, they resemble uncorrelated noise. Here, the Markovian approximation becomes physically justifiable.

This finding is analogous to theoretical results in free shear flows [35], [36], [37], where the validity of the Markovian assumption depends on the observation timescale relative to the Taylor microscale. Those studies concluded that statistics of the longitudinal velocity increments exhibit Markovian properties when scale difference approximately equals the Taylor microscale. Analogously, we propose that λ serves as a critical scale for near-wall turbulence, dictating whether the flow structure is sufficiently resolved to require non-Markovian modeling or sufficiently quasi-random to admit a Markovian approximation.

Finally, we note that the application of the Markovian approximation is dependent on specific boundary conditions. We assumed a hydrodynamically smooth wall. However, surface roughness is expected to reduce the sublayer thickness [75], potentially altering the frequency of coherent structures. Furthermore, the assumption of a one-way coupling regime neglects feedback mechanisms where, at higher concentrations, particles intensify sweep and ejection events [76], creating a coupled

system likely requiring non-Markovian descriptions. Additionally, for phenomena occurring higher in the boundary layer, such as particle deposition and sedimentation, the influence of large-scale structures is more pronounced. Recent work by Hung and Tsai [63] demonstrated that a non-Markovian model was superior to a Markovian one for reconstructing sedimentation measurements, utilizing a much lower decay rate ($\lambda \approx 0.02$) consistent with the stronger intermittency of the buffer layer. Thus, while the Markovian approximation can be tuned to work for simple sublayer resuspension, the non-Markovian framework offers a generalized, physically grounded description essential for complex, memory-dependent flows.

4. Conclusion

This study investigates the validity of the Markovian assumption for modeling near-wall turbulence dynamics, by investigating the detachment of micron-sized particles from the viscous sublayer as a test case. While classical theoretical frameworks typically model turbulent velocity increments as memoryless (Markovian) processes consistent with Kolmogorov's K41 hypothesis, we hypothesized that the presence of coherent structures necessitates a non-Markovian description accounting for flow memory and intermittency, consistent with the refined K62 theory.

To test this hypothesis, we developed a theoretical-numerical framework coupling a Lagrangian stochastic model with a fOUP. The physical inputs for this model, specifically the Hurst exponent and event decay rates, were derived from a DNS of a fully developed turbulent channel flow. Our analysis of the WSS signal revealed that while the occurrence of high- and low-drag events follows Poissonian statistics, the dynamics within these events exhibit strong persistence ($H \approx 0.84$). This finding

provides physical evidence that the flow characteristics within the viscous sublayer are temporally correlated.

A central finding in this work is the physical justification of the Markovian approximation through the lens of our non-Markovian framework. Comparative simulations reveal that the empirical success of classical Markovian models does not stem from an accurate description of the instantaneous flow topology, but rather from the capacity of their free parameters, to act as a phenomenological surrogate for flow memory. We demonstrate that when C_0 is tuned to match the integrated energy of the persistent structures explicitly resolved by our non-Markovian formulation, the macroscopic predictions of the two frameworks converge. This implies that previous Markovian studies have effectively, albeit implicitly, modeled the influence of coherent structures by adjusting the intensity of the stochastic forcing.

Furthermore, by formulating a general non-Markovian framework, we established the validity limits of this approximation by identifying a critical regime transition governed by the event decay rate, λ . We found that for strong intermittency ($\lambda < 0.2$), where coherent structures exhibit extended temporal coherence, the Markovian approximation fails to capture the sustained forcing required for detachment and a non-Markovian modeling framework is imperative. Conversely, for weak intermittency ($\lambda > 0.2$), structures decay sufficiently rapidly to be treated as quasi-random noise, rendering the Markovian assumption physically justifiable. Thus, this study concludes that the validity of the Markovian approximation in near-wall turbulence is determined by the ratio of the structural decay time to the particle response time, establishing $\lambda = 0.2$ as a threshold for transition between Markovian and non-Markovian regime.

CRediT authorship contribution statement

David Ben Shlomo: Writing – original draft, Writing – review & editing, Conceptualization, Formal analysis, Investigation, Data curation. **Ronen Berkovich:** Writing – original draft, Writing – review & editing, Conceptualization, Formal analysis, Investigation, Funding acquisition, Supervision. **Eyal Fattal:** Writing – original draft, Writing – review & editing, Conceptualization, Formal analysis, Investigation, Funding acquisition, Supervision.

Declaration of competing interests

The authors declare that they have no known competing financial interests or personal relationships that could have appeared to influence the work reported in this paper.

Data availability

Data will be made available on request.

Acknowledgments

The authors wish to thank Ziv Klausner and Yehuda Arav for helpful discussions. The authors of this work are grateful for the generous support of Pazy Foundation, grant ID 133-2020 and the John R. Goldsmith Memorial Prize Fund.

References

- [1] J. Jiménez, “Coherent structures in wall-bounded turbulence,” *J. Fluid Mech.*, vol. 842, p. P1, May 2018, doi: 10.1017/jfm.2018.144.

- [2] S. B. Pope, *Turbulent Flows*. Cambridge University Press, 2000. doi: 10.1017/CBO9780511840531.
- [3] A. N. Kolmogorov, “Local structure of turbulence in an incompressible viscous fluid at very large Reynolds numbers,” *Dokl Akad Nauk SSSR*, vol. 30, no. 4, pp. 299–301, 1941.
- [4] C. Henry, J.-P. Minier, and S. Brambilla, “Particle resuspension: Challenges and perspectives for future models,” *Phys. Rep.*, vol. 1007, pp. 1–98, Mar. 2023, doi: 10.1016/j.physrep.2022.12.005.
- [5] C. Henry and J. P. Minier, “Progress in particle resuspension from rough surfaces by turbulent flows,” *Prog. Energy Combust. Sci.*, vol. 45, no. C, 2014, doi: 10.1016/j.pecs.2014.06.001.
- [6] J. Qian, J. Peccia, and A. R. Ferro, “Walking-induced particle resuspension in indoor environments,” *Atmos. Environ.*, vol. 89, pp. 464–481, Jun. 2014, doi: 10.1016/j.atmosenv.2014.02.035.
- [7] M. W. Reeks and D. Hall, “Kinetic models for particle resuspension in turbulent flows: theory and measurement,” *J. Aerosol Sci.*, vol. 32, no. 1, pp. 1–31, Jan. 2001, doi: 10.1016/S0021-8502(00)00063-X.
- [8] C. Henry, J. P. Minier, and G. Lefèvre, “Numerical study on the adhesion and reentrainment of nondeformable particles on surfaces: The role of surface roughness and electrostatic forces,” *Langmuir*, vol. 28, no. 1, pp. 438–452, Jan. 2012, doi: 10.1021/la203659q.
- [9] M. Guingo and J. P. Minier, “A new model for the simulation of particle resuspension by turbulent flows based on a stochastic description of wall roughness and adhesion forces,” *J. Aerosol Sci.*, vol. 39, no. 11, 2008, doi: 10.1016/j.jaerosci.2008.06.007.

- [10] A. J. Sutherland, “Proposed mechanism for sediment entrainment by turbulent flows,” *J. Geophys. Res. 1896-1977*, vol. 72, no. 24, pp. 6183–6194, Dec. 1967, doi: <https://doi.org/10.1029/JZ072i024p06183>.
- [11] J. W. Cleaver and B. Yates, “Mechanism of detachment of colloidal particles from a flat substrate in a turbulent flow,” *J. Colloid Interface Sci.*, vol. 44, no. 3, pp. 464–474, Sep. 1973, doi: [10.1016/0021-9797\(73\)90323-8](https://doi.org/10.1016/0021-9797(73)90323-8).
- [12] A. H. Ibrahim, R. M. Brach, and P. F. Dunn, “Microparticle detachment from surfaces exposed to turbulent air row: microparticle motion after detachment,” *Aerosol Sci.*, vol. 35, pp. 1189–1204, 2004, doi: [10.1016/j.jaerosci.2004.05.003](https://doi.org/10.1016/j.jaerosci.2004.05.003).
- [13] Y. Jiang, S. Matsusaka, H. Masuda, and Y. Qian, “Characterizing the effect of substrate surface roughness on particle-wall interaction with the airflow method,” *Powder Technol.*, vol. 186, no. 3, pp. 199–205, Sep. 2008, doi: [10.1016/j.powtec.2007.11.041](https://doi.org/10.1016/j.powtec.2007.11.041).
- [14] M. Soltani and G. Ahmadi, “On particle adhesion and removal mechanisms in turbulent flows,” *J. Adhes. Sci. Technol.*, vol. 8, no. 7, pp. 763–785, 1994, doi: [10.1163/156856194X00799](https://doi.org/10.1163/156856194X00799).
- [15] B. P. K. Yung, H. Merry, and T. R. Bott, “The role of turbulent bursts in particle re-entrainment in aqueous systems,” *Chem. Eng. Sci.*, vol. 44, no. 4, pp. 873–882, 1989, doi: [10.1016/0009-2509\(89\)85260-1](https://doi.org/10.1016/0009-2509(89)85260-1).
- [16] D. Kaftori, G. Hetsroni, and S. Banerjee, “Particle behavior in the turbulent boundary layer. I. Motion, deposition, and entrainment,” *Phys. Fluids*, vol. 7, no. 5, pp. 1095–1106, May 1995, doi: [10.1063/1.868551](https://doi.org/10.1063/1.868551).
- [17] D. A. Braaten, R. H. Shaw, and K. T. Paw U, “Boundary-layer flow structures associated with particle reentrainment,” *Bound.-Layer Meteorol.*, vol. 65, no. 3, pp. 255–272, Aug. 1993, doi: [10.1007/BF00705529](https://doi.org/10.1007/BF00705529).

- [18] R. van Hout, “Spatially and temporally resolved measurements of bead resuspension and saltation in a turbulent water channel flow,” *J. Fluid Mech.*, vol. 715, pp. 389–423, Jan. 2013, doi: 10.1017/jfm.2012.525.
- [19] Y. Ninto and M. H. Garcia, “Experiments on particle—turbulence interactions in the near-wall region of an open channel flow: implications for sediment transport,” *J. Fluid Mech.*, vol. 326, pp. 285–319, Nov. 1996, doi: 10.1017/S0022112096008324.
- [20] M. Soltani and G. Ahmadi, “Direct numerical simulation of particle entrainment in turbulent channel flow,” *Phys. Fluids*, vol. 7, no. 3, pp. 647–657, Mar. 1995, doi: 10.1063/1.868587.
- [21] C. Marchioli and A. Soldati, “Mechanisms for particle transfer and segregation in a turbulent boundary layer,” *J. Fluid Mech.*, vol. 468, pp. 283–315, Oct. 2002, doi: 10.1017/S0022112002001738.
- [22] S. J. Kline, W. C. Reynolds, F. A. Schraub, and P. W. Runstadler, “The structure of turbulent boundary layers,” *J. Fluid Mech.*, vol. 30, no. 4, pp. 741–773, Dec. 1967, doi: 10.1017/S0022112067001740.
- [23] S. J. Kline and P. W. Runstadler, “Some Preliminary Results of Visual Studies of the Flow Model of the Wall Layers of the Turbulent Boundary Layer,” *J. Appl. Mech.*, vol. 26, no. 2, pp. 166–170, 1959, doi: 10.1115/1.4011977.
- [24] S. S. Kumar, X. Huang, X. Yang, and J. Hong, “Three dimensional flow motions in the viscous sublayer,” *Theor. Appl. Mech. Lett.*, vol. 11, no. 2, p. 100239, Feb. 2021, doi: 10.1016/j.taml.2021.100239.
- [25] J. M. Wallace, H. Eckelmann, and R. S. Brodkey, “The wall region in turbulent shear flow,” *J. Fluid Mech.*, vol. 54, no. 1, pp. 39–48, Jul. 1972, doi: 10.1017/S0022112072000515.

- [26] W. W. Willmarth and S. S. Lu, “Structure of the Reynolds stress near the wall,” *J. Fluid Mech.*, vol. 55, no. 1, pp. 65–92, Sep. 1972, doi: 10.1017/S002211207200165X.
- [27] R. Agrawal *et al.*, “Low- and High-Drag Intermittencies in Turbulent Channel Flows,” *Entropy*, vol. 22, no. 10, p. 1126, Oct. 2020, doi: 10.3390/e22101126.
- [28] P. Lenaers, Q. Li, G. Brethouwer, P. Schlatter, and R. Örlü, “Rare backflow and extreme wall-normal velocity fluctuations in near-wall turbulence,” *Phys. Fluids*, vol. 24, no. 3, p. 035110, Mar. 2012, doi: 10.1063/1.3696304.
- [29] C. E. Willert *et al.*, “Experimental evidence of near-wall reverse flow events in a zero pressure gradient turbulent boundary layer,” *Exp. Therm. Fluid Sci.*, vol. 91, pp. 320–328, Feb. 2018, doi: 10.1016/j.expthermflusci.2017.10.033.
- [30] B. Guerrero, M. F. Lambert, and R. C. Chin, “Precursors of backflow events and their relationship with the near-wall self-sustaining process,” *J. Fluid Mech.*, vol. 933, p. A33, Feb. 2022, doi: 10.1017/jfm.2021.1082.
- [31] B. Guerrero, M. F. Lambert, and R. C. Chin, “Extreme wall shear stress events in turbulent pipe flows: spatial characteristics of coherent motions,” *J. Fluid Mech.*, vol. 904, p. A18, Dec. 2020, doi: 10.1017/jfm.2020.689.
- [32] D. Ben Shlomo, R. Almog, Z. Klausner, E. Fattal, and R. Berkovich, “Introducing surface roughness in adhesion for stochastic and Rock’n’Roll models to describe particle resuspension in turbulent flows,” *Surf. Interfaces*, vol. 48, p. 104321, May 2024, doi: 10.1016/j.surfin.2024.104321.
- [33] S. C. Fu, C. Y. H. Chao, R. M. C. So, and W. T. Leung, “Particle resuspension in a wall-bounded turbulent flow,” *J. Fluids Eng. Trans. ASME*, vol. 135, no. 4, 2013, doi: 10.1115/1.4023660.

- [34] R. Hu, P. L. Johnson, and C. Meneveau, “Modeling the resuspension of small inertial particles in turbulent flow over a fractal-like multiscale rough surface,” *Phys. Rev. Fluids*, vol. 8, no. 2, p. 024304, Feb. 2023, doi: 10.1103/PhysRevFluids.8.024304.
- [35] C. Renner, J. Peinke, and R. Friedrich, “Experimental indications for Markov properties of small-scale turbulence,” *J. Fluid Mech.*, vol. 433, pp. 383–409, Apr. 2001, doi: 10.1017/S0022112001003597.
- [36] R. Stresing, J. Peinke, R. E. Seoud, and J. C. Vassilicos, “Defining a New Class of Turbulent Flows,” *Phys. Rev. Lett.*, vol. 104, no. 19, p. 194501, May 2010, doi: 10.1103/PhysRevLett.104.194501.
- [37] Ch. Renner, “Universality of Small Scale Turbulence,” *Phys. Rev. Lett.*, vol. 89, no. 12, 2002, doi: 10.1103/PhysRevLett.89.124502.
- [38] A. N. Kolmogorov, “A refinement of previous hypotheses concerning the local structure of turbulence in a viscous incompressible fluid at high Reynolds number,” *J. Fluid Mech.*, vol. 13, no. 1, pp. 82–85, 1962, doi: 10.1017/S0022112062000518.
- [39] I. Marusic, R. Mathis, and N. Hutchins, “Predictive Model for Wall-Bounded Turbulent Flow,” *Science*, vol. 329, no. 5988, pp. 193–196, Jul. 2010, doi: 10.1126/science.1188765.
- [40] R. Örlü and P. Schlatter, “On the fluctuating wall-shear stress in zero pressure-gradient turbulent boundary layer flows,” *Phys. Fluids*, vol. 23, no. 2, p. 021704, Feb. 2011, doi: 10.1063/1.3555191.
- [41] J. Graham *et al.*, “A Web services accessible database of turbulent channel flow and its use for testing a new integral wall model for LES,” *J. Turbul.*, vol. 17, no. 2, pp. 181–215, Feb. 2016, doi: 10.1080/14685248.2015.1088656.

- [42] Y. Li *et al.*, “A public turbulence database cluster and applications to study Lagrangian evolution of velocity increments in turbulence,” *J. Turbul.*, vol. 9, p. N31, Jan. 2008, doi: 10.1080/14685240802376389.
- [43] S. Balachandar and J. K. Eaton, “Turbulent Dispersed Multiphase Flow,” *Annu. Rev. Fluid Mech.*, vol. 42, no. Volume 42, 2010, pp. 111–133, Jan. 2010, doi: 10.1146/annurev.fluid.010908.165243.
- [44] S. Elghobashi, “On predicting particle-laden turbulent flows,” *Appl. Sci. Res.*, vol. 52, no. 4, pp. 309–329, Jun. 1994, doi: 10.1007/BF00936835.
- [45] G. Quibeuf, F. Charru, and L. Lacaze, “Particle motion within the viscous sublayer of a turbulent shear flow,” *Phys. Rev. Fluids*, vol. 5, no. 1, p. 014306, Jan. 2020, doi: 10.1103/PhysRevFluids.5.014306.
- [46] R. D. Whalley, D. J. C. Dennis, M. D. Graham, and R. J. Poole, “An experimental investigation into spatiotemporal intermittencies in turbulent channel flow close to transition,” *Exp. Fluids*, vol. 60, no. 6, Jun. 2019, doi: 10.1007/s00348-019-2739-9.
- [47] A. S. Pereira, R. L. Thompson, and G. Mompean, “Common features between the Newtonian laminar–turbulent transition and the viscoelastic drag-reducing turbulence,” *J. Fluid Mech.*, vol. 877, pp. 405–428, Oct. 2019, doi: 10.1017/jfm.2019.567.
- [48] J. Mielniczuk and P. Wojdyłło, “Estimation of Hurst exponent revisited,” *Comput. Stat. Data Anal.*, vol. 51, no. 9, pp. 4510–4525, May 2007, doi: 10.1016/j.csda.2006.07.033.
- [49] P. Abry, P. Flandrin, M. S. Taqqu, and D. Veitch, “Wavelets for the Analysis, Estimation, and Synthesis of Scaling Data,” in *Self-Similar Network Traffic and*

Performance Evaluation, John Wiley & Sons, Ltd, 2000, pp. 39–88. doi: 10.1002/047120644X.ch2.

[50] R. M. Bryce and K. B. Sprague, “Revisiting detrended fluctuation analysis,” *Sci. Rep.*, vol. 2, no. 1, p. 315, Mar. 2012, doi: 10.1038/srep00315.

[51] Y.-J. Hung and C. W. Tsai, “Application of stochastic models for long-range sediment transport during extreme typhoon events,” *J. Hydrol. Reg. Stud.*, vol. 60, p. 102463, Aug. 2025, doi: 10.1016/j.ejrh.2025.102463.

[52] G. Ziskind, “Particle resuspension from surfaces: Revisited and re-evaluated,” *Rev. Chem. Eng.*, vol. 22, pp. 1–123, Jan. 2006, doi: 10.1515/REVCE.2006.22.1-2.1.

[53] M. Soltani and G. Ahmadi, “On particle adhesion and removal mechanisms in turbulent flows,” *J. Adhes. Sci. Technol.*, vol. 8, no. 7, pp. 763–785, Jan. 1994, doi: 10.1163/156856194X00799.

[54] G. G. Stokes, “On the effect of the internal friction of fluids on the motion of pendulums,” 1851.

[55] M. E. O’Neill, “A sphere in contact with a plane wall in a slow linear shear flow,” *Chem. Eng. Sci.*, vol. 23, no. 11, 1968, doi: 10.1016/0009-2509(68)89039-6.

[56] A. M. Mollinger and F. T. M. Nieuwstadt, “Measurement of the lift force on a particle fixed to the wall in the viscous sublayer of a fully developed turbulent boundary layer,” *J. Fluid Mech.*, vol. 316, pp. 285–306, Jun. 1996, doi: 10.1017/S0022112096000547.

[57] A. D. Maude, “The movement of a sphere in front of a plane at low Reynolds number,” *Br. J. Appl. Phys.*, vol. 14, no. 12, p. 894, Dec. 1963, doi: 10.1088/0508-3443/14/12/316.

[58] Y. I. Rabinovich, J. J. Adler, A. Ata, R. K. Singh, and B. M. Moudgil, “Adhesion between nanoscale rough surfaces: II. Measurement and comparison with theory,” *J. Colloid Interface Sci.*, vol. 232, no. 1, pp. 17–24, Dec. 2000, doi: 10.1006/jcis.2000.7168.

[59] H. Risken, *The Fokker-Planck Equation*, vol. 18. in Springer Series in Synergetics, vol. 18. Berlin, Heidelberg: Springer, 1989. doi: 10.1007/978-3-642-61544-3.

[60] G. E. Uhlenbeck and L. S. Ornstein, “On the Theory of the Brownian Motion,” *Phys. Rev.*, vol. 36, no. 5, pp. 823–841, Sep. 1930, doi: 10.1103/PhysRev.36.823.

[61] D. Faranda *et al.*, “Modelling and analysis of turbulent datasets using Auto Regressive Moving Average processes,” *Phys. Fluids*, vol. 26, no. 10, p. 105101, Oct. 2014, doi: 10.1063/1.4896637.

[62] P. Cheridito, H. Kawaguchi, and M. Maejima, “Fractional Ornstein-Uhlenbeck processes,” *Electron. J. Probab.*, vol. 8, no. none, pp. 1–14, Jan. 2003, doi: 10.1214/EJP.v8-125.

[63] Y.-J. Hung and C. W. Tsai, “Modeling memory-enhanced stochastic suspended sediment transport with fractional Brownian motion in time-persistent turbulent flow,” *Stoch. Environ. Res. Risk Assess.*, vol. 38, no. 11, pp. 4555–4575, Nov. 2024, doi: 10.1007/s00477-024-02818-9.

[64] S. W. Shen and C. W. Tsai, “Incorporating memory effect into a fractional stochastic diffusion particle tracking model for suspended sediment using Malliavin-Calculus-based fractional Brownian Motion,” *Chaos Solitons Fractals*, vol. 187, p. 115312, Oct. 2024, doi: 10.1016/j.chaos.2024.115312.

[65] C. W. Tsai, S.-H. Huang, and S. Y. Hung, “Incorporating the Memory Effect of Turbulence Structures Into Suspended Sediment Transport Modeling,” *Water Resour. Res.*, vol. 57, no. 3, p. e2020WR028475, 2021, doi: 10.1029/2020WR028475.

[66] B. B. Mandelbrot and J. W. Van Ness, “Fractional Brownian Motions, Fractional Noises and Applications,” *SIAM Rev.*, vol. 10, no. 4, pp. 422–437, 1968.

[67] J. L. McCauley, “Non-Markov stochastic processes satisfying equations usually associated with a Markov process,” *Eur. Phys. J. Spec. Top.*, vol. 204, no. 1, pp. 133–143, Apr. 2012, doi: 10.1140/epjst/e2012-01557-7.

[68] C. E. Willert and J. Klinner, “Dynamic wall shear stress measurement using event-based 3d particle tracking,” *Exp. Fluids*, vol. 66, no. 2, p. 32, Jan. 2025, doi: 10.1007/s00348-024-03946-2.

[69] S. Tardu, *Transport and coherent structures in wall turbulence*. John Wiley & Sons, 2014.

[70] S. Tardu, *Statistical Approach to Wall Turbulence*. John Wiley & Sons, 2013.

[71] R. J. Adrian, “Hairpin vortex organization in wall turbulence,” *Phys. Fluids*, vol. 19, no. 4, p. 041301, Apr. 2007, doi: 10.1063/1.2717527.

[72] S. K. Robinson, “Coherent Motions in the Turbulent Boundary Layer,” *Annu. Rev. Fluid Mech.*, vol. 23, no. 1, pp. 601–639, 1991, doi: 10.1146/annurev.fl.23.010191.003125.

[73] Y. Liu, M. Klaas, and W. Schröder, “Measurements of the wall-shear stress distribution in turbulent channel flow using the micro-pillar shear stress sensor MPS3,” *Exp. Therm. Fluid Sci.*, vol. 106, pp. 171–182, Sep. 2019, doi: 10.1016/j.expthermflusci.2019.04.022.

- [74] C. Xu, Z. Zhang, J. M. J. den Toonder, and F. T. M. Nieuwstadt, “Origin of high kurtosis levels in the viscous sublayer. Direct numerical simulation and experiment,” *Phys. Fluids*, vol. 8, no. 7, pp. 1938–1944, Jul. 1996, doi: 10.1063/1.868973.
- [75] A. J. Grass, “Structural features of turbulent flow over smooth and rough boundaries,” *J. Fluid Mech.*, vol. 50, no. 2, pp. 233–255, Nov. 1971, doi: 10.1017/S0022112071002556.
- [76] K. Luo, H. Zhang, M. Luo, X. Wu, and J. Fan, “Effects of solid particles and wall roughness on turbulent boundary layer in a two-phase horizontal channel flow,” *Powder Technol.*, vol. 353, pp. 48–56, Jul. 2019, doi: 10.1016/j.powtec.2019.05.009.

Supplementary data

for

On the Markovian assumption in near-wall turbulence: The case of particle resuspension

David Ben-Shlomo^{1,2}, Ronen Berkovich^{1,3,*}, Eyal Fattal^{2,*}

¹Department of Chemical Engineering, Ben-Gurion University of the Negev, Beer-Sheva 8410501, Israel

²Department of Applied Mathematics, Israel Institute for Biological Research, Ness-Ziona 7410001, Israel

³Ilze Katz Institute for Nanoscience and Technology, Ben-Gurion University of the Negev, Beer-Sheva 8410501, Israel

1. Influence of the Hurst exponent on particle dynamics

The fractional Brownian motion (fBm) generalizes classical Brownian motion by allowing correlated increments. It is characterized by a zero mean $\langle B^H(t) \rangle = 0$, a variance $\langle (B^H(t))^2 \rangle = t^{2H}$, and a covariance $\langle B^H(s)B^H(t) \rangle = \frac{1}{2}(|s|^{2H} + |t|^{2H} - |t - s|^{2H})$. The fBm can be represented as a cumulative integral of a Gaussian random process:

$$B^H(t) = \frac{1}{\Gamma(H + \frac{1}{2})} \int_{-\infty}^0 \left[(t - s)^{H - \frac{1}{2}} - (-s)^{H - \frac{1}{2}} \right] dW(s) + \frac{1}{\Gamma(H + \frac{1}{2})} \int_0^t (t - s)^{H - \frac{1}{2}} dW(s) \quad (S1)$$

where $\Gamma(H)$ is the gamma function [1]. The exponent H is a real number in $(0, 1)$ and governs the memory properties of the process. Specifically, for $H = 0.5$, the standard Wiener process is recovered. For $0 < H < 0.5$ the process exhibits anti-persistence, meaning that increases are likely to be followed by decreases and vice versa. Conversely, for $0.5 < H < 1$, the process is persistent, with trends tending to continue

in the same direction. The rescaled range (R/S) method, developed by Hurst [2], is expressed as

$$\log(R/S) = \log(c) + H\log(n) \quad (S2)$$

where R is the adjusted range, S is the standard deviation, c is a constant, H is the Hurst exponent and n is the sample length. Equation (S2) is linear in its current form, allowing the Hurst exponent H to be obtained through a linear regression of the data.

To illustrate the influence of the Hurst exponent on particle dynamics, figure S1 presents a comparison of 1,000 sample paths and their correlation generated for various values of H , obtained by numerically solving equation (S1) using the Cholesky decomposition method [3]. The trajectories are plotted together with their ensemble mean and standard deviation. As expected from their definitions, both the Wiener process ($H = 0.5$) and fBm processes exhibit zero ensemble mean. Additionally, as the Hurst exponent increases, the trajectories display greater spatial extent. For $H > 0.5$, the sample paths exhibit positively correlated, smoother behavior with enhanced persistence, enabling them to traverse significantly larger distances due to their dependent increments. Notably, the difference in magnitude between the Wiener ($H = 0.5$) and fBm with $H = 0.8$ processes can reach up to an order of magnitude. These characteristics are also emphasized in the normalized covariance by the product of standard deviations of each H value. In case of the Wiener process ($H = 0.5$), the normalized covariance structure reduces to the Brownian case, which decays proportionally to the smaller time. For persistent behavior ($H > 0.5$), The normalized covariance remains high even far off the diagonal, indicating long memory. For anti-persistent behavior ($H < 0.5$), the normalized covariance decays quickly off the diagonal, values at distant times become nearly uncorrelated.

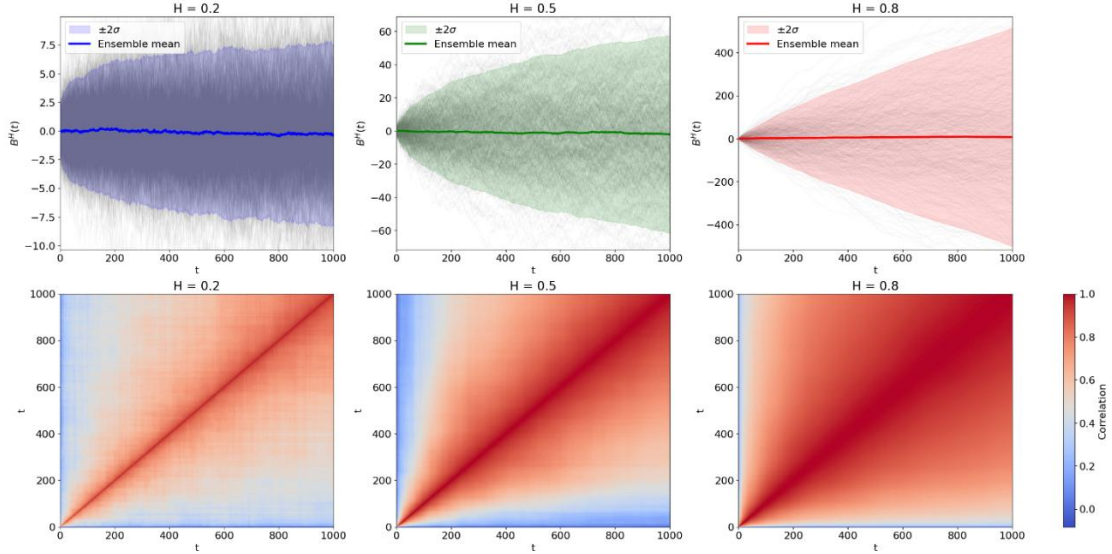


Fig. S1. Top: sample paths (trajectories) of fBm for three different Hurst exponents: $H = 0.2$ (blue) $H = 0.5$ (green) $H = 0.8$ (red), based on 1,000 realizations each. Bottom: correlation heat map corresponding for the different Hurst exponent values. The correlation here is the normalized covariance by the product of standard deviations. Both the time variable t and the fBm values $\mathbf{B}^H(t)$ are dimensionless.

2. Numerical simulation procedure

The non-Markovian simulation proceeds as follows. At the start of the simulation, the particle is set to rest on the surface. At each subsequent time step, Δt , the particle may encounter a high- or low-drag event associated with turbulent coherent structures. The probability of encountering such an event is determined from the event frequency analysis performed on direct numerical simulation (DNS) data. If the particle encounters an event, the fluctuating angular velocity is computed using the fractional Ornstein-Uhlenbeck process (fOUP), with both the Hurst exponent and the event duration derived from the DNS-based analysis conducted in this study. In the absence of an event, the fluctuating velocity is calculated using the classical Ornstein-Uhlenbeck process (OUP), consistent with Markovian dynamics. The total angular

velocity of the particle, obtained as the sum of the mean and fluctuating contributions following Reynolds decomposition, is then compared to the critical resuspension threshold, ω_c . If the total angular velocity exceeds the critical value, the particle is considered to overcome the adhesive forces and is assumed to be resuspended. Otherwise, the particle remains on the surface, and the simulation proceeds to the next time step, repeating the same procedure iteratively.

The integration of both the OUP and fOUP was performed using the Euler scheme, which has been previously demonstrated to be a simple and reliable method for solving stochastic differential equations [4], [5]. It is further emphasized that, since the stochastic term in the Langevin equation is independent of the solved variable (ω' in this case), the integration of the stochastic differential equation is straightforward and the Itô-Stratonovich dilemma does not apply [6]. The simulation time step was selected to be equal to the turbulent integral timescale, $T_0 = \nu/u_\tau^2$, which is two orders of magnitude smaller than the average bursting interval ($300\nu/u_\tau^2$) [7] and one order smaller than the integral timescale within the viscous sublayer ($20\nu/u_\tau^2$) for the streamwise wall shear stress [8], ensuring adequate temporal resolution to sample the memory effect. The total simulation duration was set for one second, reflecting the short timescale of the resuspension process, which occurs on the order of milliseconds [4]. Each simulation tracks 1,000 particles, a number determined through sensitivity analyses showing that increasing the particle count does not alter the predicted resuspended fraction, thereby confirming statistical significance. Other simulation parameters remain consistent with those defined in [4], [9]. Finally, owing to the limited variation of the Hurst exponent obtained from the rescaled range analysis, and the demonstrated insensitivity of the resuspension results to this variation, the

single representative value $H = 0.84$ (the median from the analysis) was adopted in the numerical algorithm of the non-Markovian model.

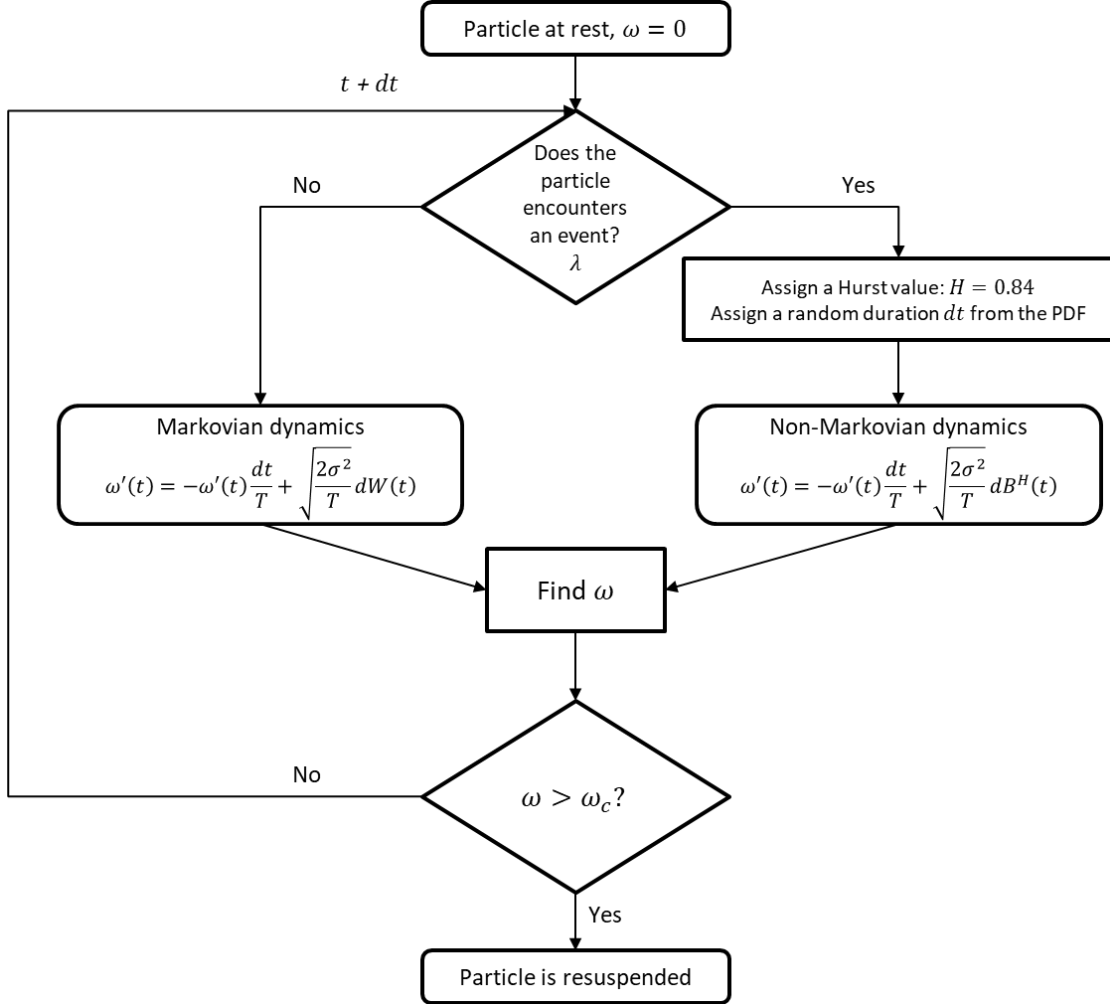


Fig. S2. Simulation algorithm flowchart.

References

- [1] B. B. Mandelbrot and J. W. Van Ness, “Fractional Brownian Motions, Fractional Noises and Applications,” *SIAM Rev.*, vol. 10, no. 4, pp. 422–437, 1968.
- [2] H. E. Hurst, “Long-Term Storage Capacity of Reservoirs,” *Trans. Am. Soc. Civ. Eng.*, vol. 116, no. 1, pp. 770–799, Jan. 1951, doi: 10.1061/TACEAT.0006518.

- [3] W. H. Press, S. A. Teukolsky, W. T. Vetterling, and B. P. Flannery, *Numerical recipes 3rd edition: The art of scientific computing*. Cambridge university press, 2007.
- [4] S. C. Fu, C. Y. H. Chao, R. M. C. So, and W. T. Leung, “Particle resuspension in a wall-bounded turbulent flow,” *J. Fluids Eng. Trans. ASME*, vol. 135, no. 4, 2013, doi: 10.1115/1.4023660.
- [5] J. P. Minier and E. Peirano, “The pdf approach to turbulent polydispersed two-phase flows,” *Phys. Rep.*, vol. 352, no. 1–3, pp. 1–214, Oct. 2001, doi: 10.1016/S0370-1573(01)00011-4.
- [6] N. G. van Kampen, “Itô versus Stratonovich,” *J. Stat. Phys.*, vol. 24, no. 1, pp. 175–187, Jan. 1981, doi: 10.1007/BF01007642.
- [7] R. F. Blackwelder and J. H. Haritonidis, “Scaling of the bursting frequency in turbulent boundary layers,” *J. Fluid Mech.*, vol. 132, pp. 87–103, Jul. 1983, doi: 10.1017/S0022112083001494.
- [8] M. Quadrio and P. Luchini, “Integral space–time scales in turbulent wall flows,” *Phys. Fluids*, vol. 15, no. 8, pp. 2219–2227, Aug. 2003, doi: 10.1063/1.1586273.
- [9] D. Ben Shlomo, R. Almog, Z. Klausner, E. Fattal, and R. Berkovich, “Introducing surface roughness in adhesion for stochastic and Rock’n’Roll models to describe particle resuspension in turbulent flows,” *Surf. Interfaces*, vol. 48, p. 104321, May 2024, doi: 10.1016/j.surfin.2024.104321.